SOME SUBTLETIES CONCERNING FLUID FLOW AND TURBULENCE MODELING IN 4-VALVE ENGINES

by

Zoran S. JOVANOVIĆ [a*], ***Branislav S. BASARA*** [b], ***Miroljub V. TOMIĆ*** [c], ***and Velimir S. PETROVIĆ*** [d]

[a] Department for IC Engines and Vehicles, Vinča Institute of Nuclear Sciences, University of Belgrade, Belgrade, Serbia
[b] AVL LIST GmbH, Graz, Austria
[c] Department for IC Engines, Faculty of Mechanical Engineering, University of Belgrade, Belgrade, Serbia
[d] Institute IMR, Belgrade, Serbia

Original scientific paper
UDC: 621.432.3:532.517.4:519.23
DOI: 10.2298/TSCI110825104J

In this paper some results concerning the structure and evolution of fluid flow pattern during induction and compression in 4- valve engines with tilted valves were presented. Results were obtained by dint of multidimensional modeling of non-reactive flows in arbitrary geometry with moving boundaries. During induction fluid flow pattern was characterized with organized tumble motion followed by small but clearly legible deterioration in the vicinity of the bottom dead center. During compression the fluid flow pattern is entirely three-dimensional and fully controlled by vortex motion located in the central part of the chamber. In order to annihilate negative effects of tumble deterioration and to enhance swirling motion one of the intake valves was deactivated. Some positive and negative effects of such attempt were elucidated. The effect of turbulence model alteration in the case of excessive macro flows was tackled as well. Namely, some results obtained with eddy-viscosity model i. e. standard k-ε model were compared with results obtained with k-ξ-f model of turbulence in domain of 4-valve engine in-cylinder flow. Some interesting results emerged rendering impetus for further quest in the near future.

Key words: *4-valve engines, automotive flows, turbulence modelling*

Introductory remarks

It is known for a long time that various types of organized flows in combustion chamber of IC engines are of predominant importance for combustion particularly with regards to flame front shape and its propagation. Some results related to the isolated or synergic effect of squish and swirl on flame propagation in various combustion chamber layouts are already analyzed and published [1, 2] but results concerning the isolated or combined effect of the third type of organized flow *i. e.* tumble are relatively less presented

* Corresponding author; e-mail: zoranj@vinca.rs

and sometimes ambiguous [3, 4]. For instance some authors [5] studied the development of swirl and tumble in five different intake valve configurations and found that when both inlet valves are open no well defined tumble flow structure was created rendering quick vortices dissipation before the bottom dead center (BDC). In spite of the fact that tumble flow is inherent to multi-valve engines some authors have demonstrated that some 2-valve engines exhibit characteristics similar to tumble flow [6, 7]. In addition, the fairly similar fluid flow patterns in the vicinity of BDC in various combustion chamber geometries yield entirely different fluid flow patterns, spatial distribution of kinetic energy of turbulence and integral length scales of turbulence in the vicinity of the top dead center (TDC) [8]. In such occasions the significance of organized tumble flow is fairly relative. Some theoretical and experimental results show that tumble is of prime importance for specific power and fuel economy increase in modern engines with multi-valve systems. The beneficial effects of tumble on CO, CH, and NO_x were also demonstrated. From the theory of turbulence is known that vortex filament subjected to compression reduces its length and promotes rotation around its axis yielding the movement on the larger scale ("spin-up" effect). It can be presumed that tumble pursues the same rule *i. e*. the destruction of well formed and expressive tumble during compression stroke generates the higher turbulence intensity and larger integral length scale of turbulence in the vicinity of TDC contributing to the flame kernel formation period reduction and faster flame propagation thereafter. The aforementioned logic imposes the conclusion that the most beneficial fluid flow pattern in the vicinity of BDC is well shaped high intensity tumble. Some additional objectives in this paper were qualitative and quantitative characterization of fluid flow pattern during induction and compression in a particular 4-valve engine, the analysis of the valve/port assembly from the point of compliance with presumed ideal fluid flow pattern, the effect of port deactivation and the effect of turbulence model variation on fluid flow and relevant turbulence parameters.

Model and computational method

The analysis of this type is inherent to multidimensional numerical modeling of non-reactive fluid flow and therefore it is quite logical to apply such a technique particularly due to fact that it is the only technique that encompasses the valve/port geometry layout in an explicit manner. In lieu of the fact that, in its essence, multidimensional models require initial and boundary conditions only their applications is fairly complicated and imply some assumptions and simplifications [9]. The full 3-D conservation integral form of unsteady equations governing turbulent motion of non-reactive mixture of ideal gas is solved on fine computational grid with moving boundaries (piston and valves) in physical domain (66,000-682,000 cells) by dint of two different codes [10-15]. In both cases the numerical solution method is based on a fully conservative finite volume approach. All dependent variables such as momentum, pressure, density, turbulence kinetic energy, dissipation rate, and passive scalar are evaluated at the cell centre. A second-order midpoint rule is used for integral approximation and a second order linear approximation for any value at the cell-face. A diffusion term is incorporated into the surface integral source after employment of the special interpolation practice. The convection is solved by a variety of differencing schemes (upwind or donor cell, interpolated donor cell, quasi second order differencing, central differencing, MINMOD and SMART). The rate of change is differenced by using implicit schemes *i. e*. Euler implicit scheme and three time level implicit scheme of second order accuracy. The overall solution procedure is iterative and is based on the semi-implicit method for pressure-

linked equations algorithm (SIMPLE). For the solution of a linear system of equations, a conjugate gradient type of solver (CGS) is used. Two different model of turbulence were used. The first one is nearly forty years old k-ε model based on Boussinesq's assumption which is certainly the most widely used model for engineering computations. On the contrary to some other models, such as Reynolds-stress closure model [16], its implementation is numerically robust due to simplicity of the model and at the same provides an acceptable level of accuracy for particular applications. The second one is relatively recent k-ζ-f model of turbulence *i. e.* eddy-viscosity model based on Durbin's elliptic relaxation concept [17-20]. This model solves a transport equation for the velocity scale ratio ζ instead of imaginary turbulent normal stress component. In addition, the pertinent hybrid boundary conditions were applied [21].

Results and discussion

The analysis of fluid flow pattern during induction and compression was based on a fairly complicated geometry layout presented in figs.1 and 2. Obviously, combustion chamber is constrained with dual intake and exhaust valves. In spite of the fact that it is not of crucial importance the inclination of intake and exhaust port is 20° and 22°, respectively. The basic block data sheet consists of bore/stroke ratio of 9.2/8.5 cm, inlet valve head diameter of 3.65 cm, exhaust valve diameter of 3.25 cm, squish gap of 0.115 cm, engine speed rpm = 2500 min^{-1}, and mixture quality $\lambda = 1$. It should be stated that maximum valve lift is $Li = 0.962$ cm while the other geometrical data (relative location, valve shape, *etc.*) could be seen in figs.1 and 2. In the case with simultaneous valve opening the commencement of intake valves opening was set at 15° bTDC and their closure at 195° aTDC.

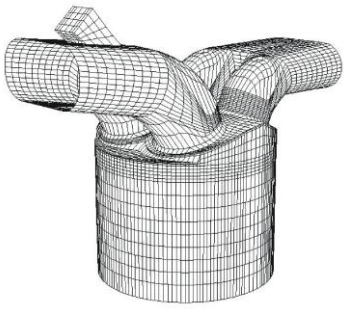

Figure 1. Perspective view of the combustion chamber geometry layout with 4-valves (upper view)

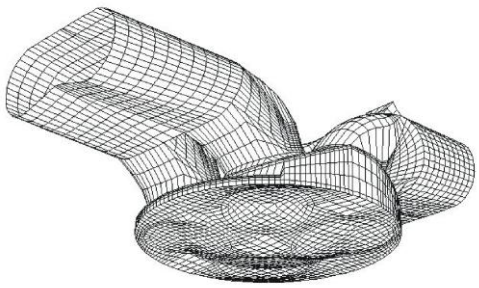

Figure 2. Perspective view of the combustion chamber geometry layout with 4-valves (bottom view)

The evolution of fluid flow pattern and turbulence was pursued in five cut planes (in x-z plane, $y = 2.1$ cm, passing through one intake and one exhaust valve, in symmetry x-z plane, $y = 0$, in y-z plane, $x = -2.1$ cm, passing through both intake valves, in y-z plane, $x = 2.1$ cm, passing through both exhaust valves and in x-y plane at $z = 8.6$ cm). The evolution of fluid flow pattern, represented as vectors, in vertical x-z plane ($y = 2.1$ cm or $y = -2.1$ cm for simultaneous valve opening) is shown in figs. 3, 4, and 5. As can be seen in fig. 3 high velocity intake jet flows over the valve, strikes upon the piston crown, curls and commences to form an elliptically-shaped vortex around y-axis in counterclockwise direction, provided

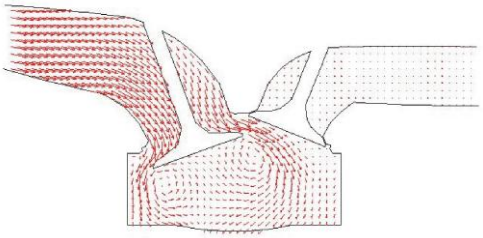

Figure 3. Fluid flow pattern in x-z plane, y = 2.1 cm, at 60° aTDC, k-ε model

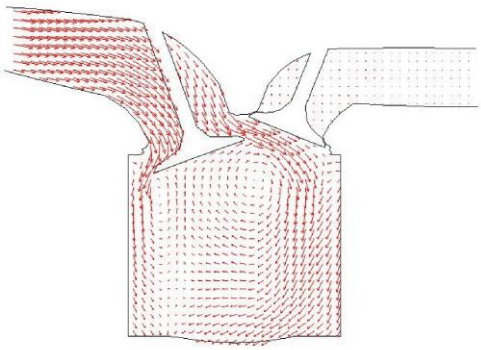

Figure 4. Perspective plot of the combustion chamber and valve/port geometry layout (squish area = 62%, cylindrical bowl) k-ε model

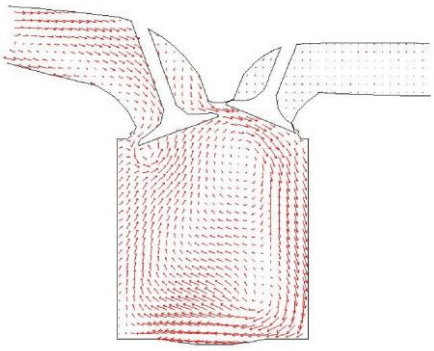

Figure 5. Fluid flow pattern in x-z plane, y = 2.1 cm, at 170° aTDC, k-ε model

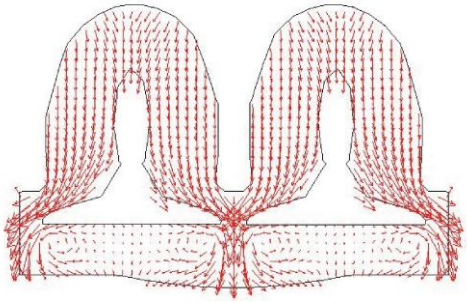

Figure 6. Fluid flow pattern in y-z plane, x = –2.1 cm, at 30° aTDC, k-ε model

that it is stipulated as such, on the left side of the valve. A small tumble-like vortex motion is created by the intake jet in clockwise direction to the right side of the valve (fig. 3).

At 60° aTDC these two vortices are of the same intensity (fig. 3) indicating the zone of coinciding flow followed by separation region just beneath the intake valve face. These two vortices are part of thoroid ring vortex that can be verified in fig. 6.

Namely, the center of rotation is equally distributed around the perimeter beneath the valve face. The increase of tumble motion intensity at maximum valve lift and further movement of piston downward exerts the attenuation of the vortex flow on the left side of intake valve. Obviously, the vortex flow is squeezed out and its shape becomes elongated (along z-axis). It's interesting to note that the center of rotation of tumble motion is in the same position. The well formed tumble flow around y-axis reduces the activity of that vortex to the zone in the vicinity of cylinder wall particularly from the moment when valve movement changes its direction (fig. 4). In the vicinity of BDC the direction of vortex flow is changed due to tumble motion and its role reduced entirely to the close proximity of intake valve face

(fig. 5). In addition, the center of rotation of tumble motion is slowly displaced to the right side of cylinder wall. Such a movement is followed by new vortex formation in the corner located adjacent to the bottom right side indicating the subtle deterioration of general tumble motion. Non-uniform distribution of tumble intensity along y-axis and two symmetric vortices in x-y plane in the vicinity of cylinder wall are responsible for the deterioration of tumble flow near BDC. Namely, as can be seen in fig. 7 the tumble intensity in vertical plane for $y = 0$ is more expressive than tumble intensity for $y = \pm 2.1$ cm. No deterioration of tumble motion in vertical plane for $y = 0$ is encountered. In addition, larger velocities are encountered in the central part of the chamber ensuing partly from jet penetration from the flanks. This activity is enhanced by vortices in x-y plane which prevent the tumble motion in vertical plane ($y = \pm 2.1$) to reach the cylinder wall. The net result is the deflection of fluid flow in y-z plane ($x = 2.1$ cm) along z-axis and formation of symmetric vortices adjacent to piston crown (fig. 8).

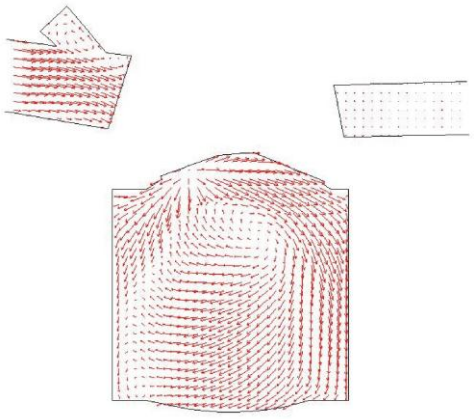

Figure 7. Fluid flow pattern in x-z plane, $y = 0$ cm, at 150° aTDC, k-ε model

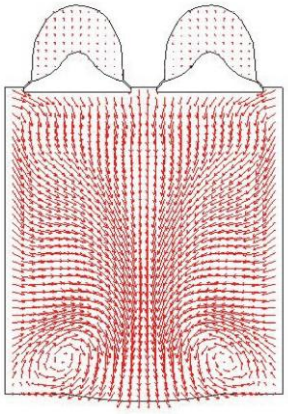

Figure 8. Fluid flow pattern in y-z plane, $x = 2.1$ cm, at 175° aTDC, k-ε model

The formation of tumble motion is observed as well through evolution of fluid flow pattern in x-y plane, as shown in figs. 9 and 10.

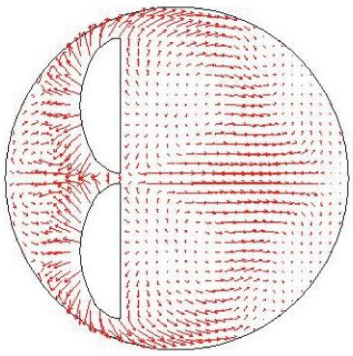

Figure 9. Fluid flow pattern in x-y plane, $z = 8.6$ cm, at 60° aTDC, k-ε model

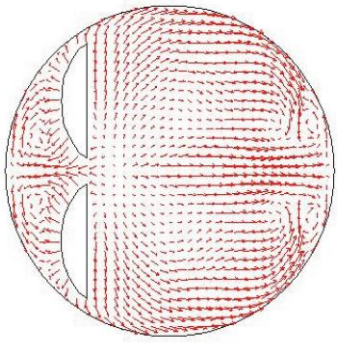

Figure 10. Fluid flow pattern in x-y plane, $z = 8.6$ cm, at 175° aTDC, k-ε model

A symmetric flow structure is created about the plane of symmetry of the cylinder head, $y = 0$, even though no conditions of symmetry were applied to the flow. It should be noted that variable visible segments of valves are due to valve movement. As can be seen in fig. 9 the synergic action of the flows over the two intake valves generates a jet traveling across the cylinder away from intake valves, formed approximately in the midway from the cylinder center to the right wall. Two counter-rotating vortices are observed on the very left side of the cylinder. Regions of low velocity magnitude are identifiable on the very right of the cylinder indicating large velocity component in z-direction. Annihilating effect of the combination of the flow is evident in the upper part of the symmetry plane (fig. 7). As can be seen in fig. 10 two counter rotating vortices are clearly legible on the very right side of the cylinder as well. The entire region is engulfed with counter rotating vortex motion in the vicinity of BDC. Namely the curling of the flow is obvious in the central part as well indicating the ingress of the fluid flow from the flank followed by deterioration of tumble motion. During compression, the quick decay of vortex motion in the zone beneath intake valves and in the vicinity of piston crown is encountered. Further movement of piston upwards yields the restitution of organized vortex motion with its center of rotation around $x = 0$. The fairly expressive w-component of the velocity in the zone of intake valves is observed rendering 1-D fluid flow thereafter. In x-z plane, $z = 8.61$ cm, on the very beginning of compression the intensive flank flows exerts detention of strong coinciding flow along x-axis, $y = 0$, and changes its direction to intake valves.

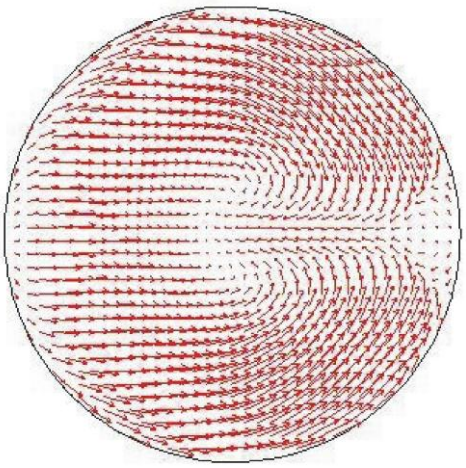

Figure 11. Fluid flow pattern in x-y plane, z = 8.6 cm, at 270° aTDC, k-ε model

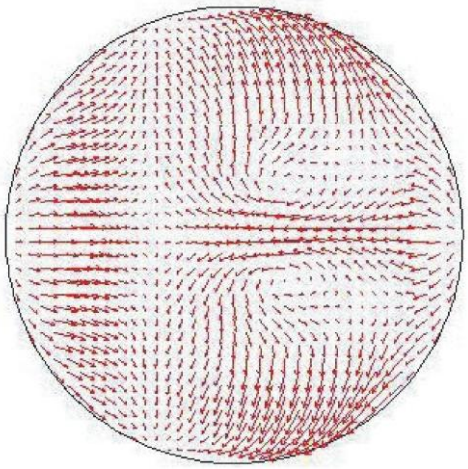

Figure 12. Fluid flow pattern in x-y plane, z = 8.6 cm, at 345° aTDC, k-ε model

High intensity coinciding flow in x-y plane is fairly similar to the fluid flow pattern in x-y plane during induction but in opposite direction (figs. 11 and 12).

Non-uniformity of fluid flow pattern along y-axis is followed by non-uniform spatial distribution of kinetic energy of turbulence along y-axis. Namely, in x-z plane, $y = -2.1$ cm, the zone with relatively high kinetic energy of turbulence is spread out through the entire region (fig. 13) while in symmetry plane, $y = 0$, the zone with high kinetic energy of turbulence is, due to strong coinciding flow (u-component dominant flow) squeezed to the zone between cylinder wall and intake valves (fig. 14).

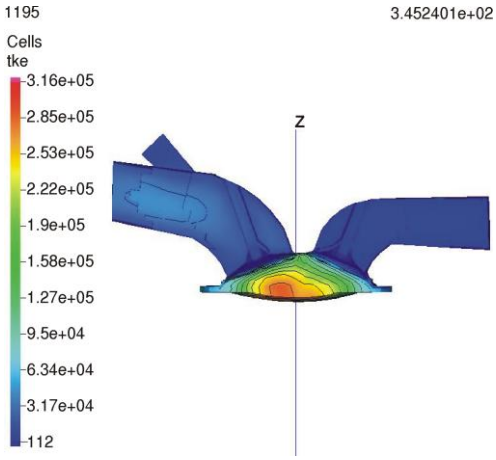

Figure 13. Spatial distribution of kinetic energy of turbulence in x-z plane, y = –2.1 cm, at 345° aTDC, k-ε model (color image see on our web site)

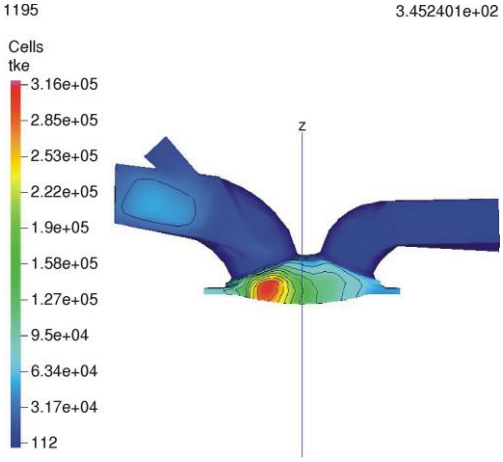

Figure 14. Spatial distribution of kinetic energy of turbulence in x-z plane, y = 0, at 345° aTDC (color image see on our web site)

Such a non-uniformity along y-axis yields characteristic and fairly inconvenient "bean-like" shape of spatial distribution of kinetic energy of turbulence in x-y plane, as can be seen in fig. 15

In order to prevent strong coinciding flow along x-axis yielding inconvenient spatial distribution of kinetic energy of turbulence in the vicinity of TDC port deactivation was included in analysis as well. The rationale for such a step is the presumption of fairly convenient mutual interaction between tumble and swirl, not observed in the case with simultaneous valve openings that could contribute to the better spatial distribution of kinetic energy of turbulence in the vicinity of TDC.

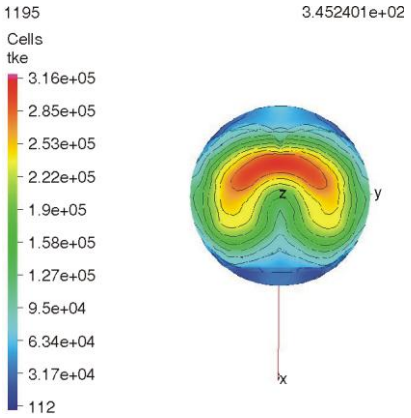

Figure 15. Spatial distribution of kinetic energy of turbulence in x-y plane, z = 8.6 cm, at 345° aTDC (color image see on our web site)

As can be seen in fig. 16 port deactivation means that one of the intake valves is kept closed and as a consequence the fluid flow pattern is entirely asymmetric. The evolution of the fluid flow in the cut-plane passing through one active and one exhaust valve is shown in figs. 17 and 18.

At the very beginning of induction the fluid flow pattern is fairly similar to the previous case (fig. 17). Namely, two counter rotating vortices around y-axis are observed as well. On the contrary to the case with both intake valves opened there is no constraint imposed by fluid flow through another intake valve and therefore no squeezing out of vortex motion in the intake valve zone is encountered. The majority of the fluid flow is directed astray and promotes vortex motions around y-axis in a set of parallel x-z planes (fig. 18 and 19). The flank flows from the zone with active intake valve promotes the formation of two concentric vortex flows around y-axis in symmetry plane, y = 0 (fig. 19). The intensity of the

inner vortex prevails and its axis of rotation gradually moves to the central part of the chamber (fig. 20) and persists there up to the end of compression stroke (fig. 21).

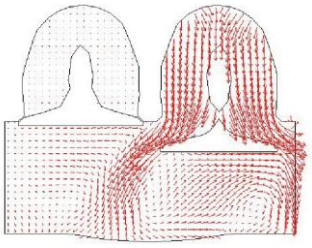

Figure 16. Fluid flow pattern in y-z plane, $x = -2.1$ cm, at 60° aTDC, port deactivation, k-ε model

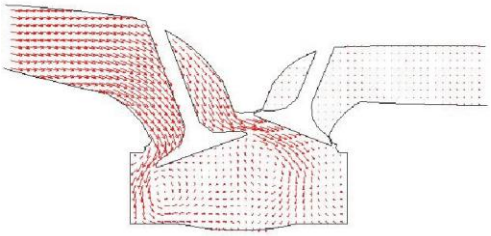

Figure 17. Fluid flow pattern in x-z plane, $y = 2.1$ cm, at 60° aTDC, port deactivation, k-ε model

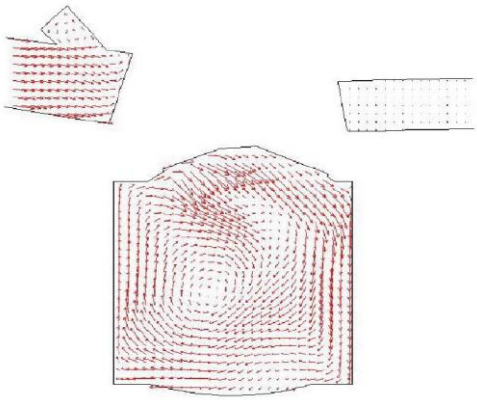

Figure 18. Fluid flow pattern in x-z plane, $y = 2.1$ cm, at 170° aTDC, port deactivation, k-ε model

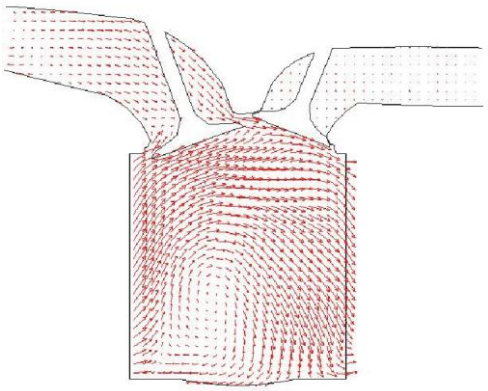

Figure 19. Fluid flow pattern in x-z plane, $y = 0$, at 120° aTDC, port deactivation, k-ε model

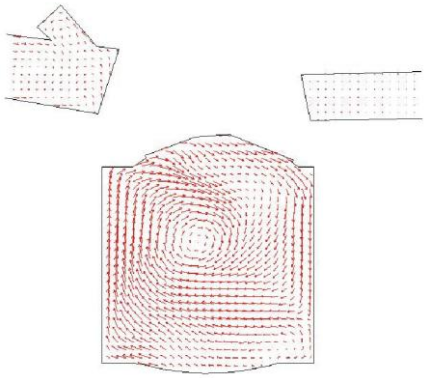

Figure 20. Fluid flow pattern in x-z plane, $y = 0$, at 170° aTDC, port deactivation, k-ε model

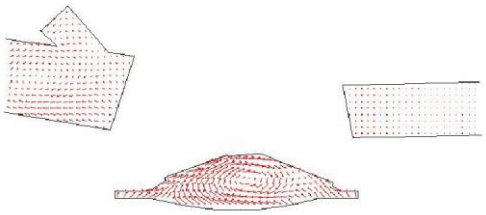

Figure 21. Fluid flow pattern in x-z plane, $y = 0$, at 345° aTDC, port deactivation, k-ε model

The evolution of the fluid flow pattern in x-z cut plane passing through inactive intake valve is shown in figs. 22 and 23.

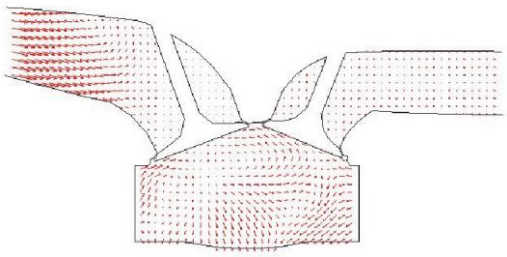

Figure 22. Fluid flow pattern in x-z plane, y = –2.1 cm, at 60° aTDC, port deactivation, k-ε model

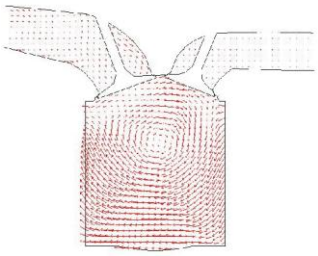

Figure 23. Fluid flow pattern in x-z plane, y = –2.1 cm, at 170° aTDC, port deactivation, k-ε model

Large soothing zones in fig. 22 indicate strong v-component velocities. In the vicinity of BDC well formed vortex motion around y-axis, similar to that in symmetry plane, y = 0, is observed as well (fig. 23).

It's interesting to note that the entire zone of inactive intake valve is engulfed with large-scale vortex motion. In addition to the vortex motion around y-axis, strong vortex motion around z-axis, in the vicinity of BDC, is encountered as well (fig. 24) being transformed, due to its increased intensity, into well formed swirling flow in the vicinity of TDC thereafter (fig. 25).

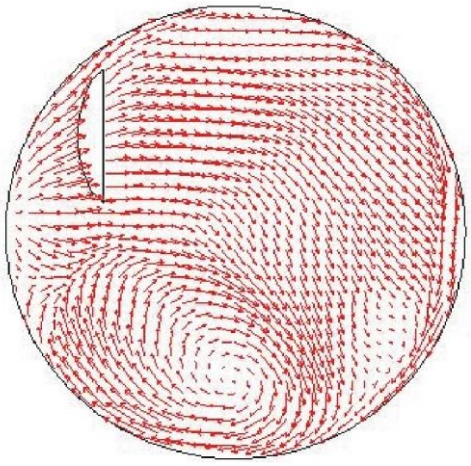

Figure 24. Fluid flow pattern in x-y plane, z = 8.6 cm, at 170° aTDC, port deactivation, k-ε model

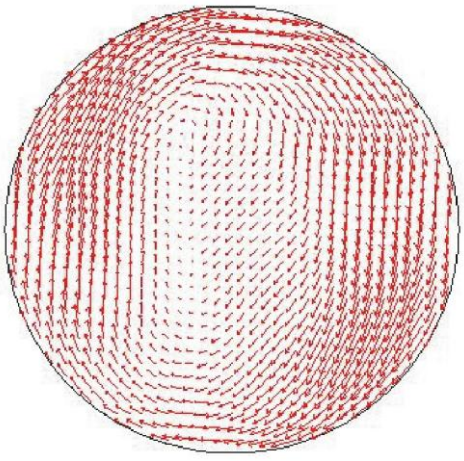

Figure 25. Fluid flow pattern in x-y plane, z = 8.6 cm, at 345° aTDC, port deactivation, k-ε model

The spatial distribution of kinetic energy of turbulence replicates entirely the fluid flow pattern and is shown in figs. 26 and 27.

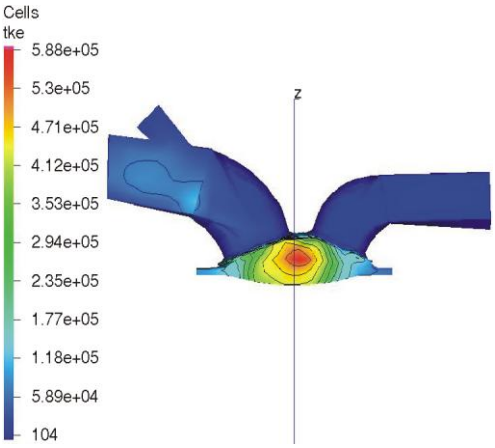

Figure 26. Spatial distribution of kinetic energy of turbulence in x-z plane, y = 0, at 345° aTDC, port deactivation, k-ε model (color image see on our web site)

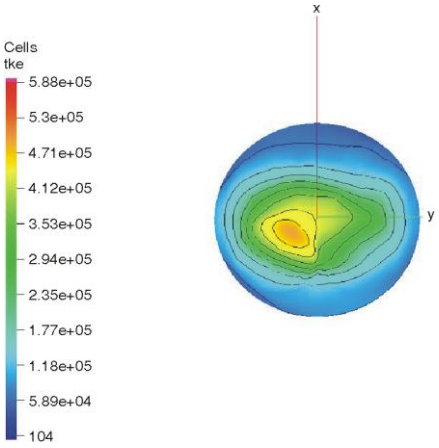

Figure 27. Spatial distribution of kinetic energy of turbulence in x-y plane, z = 8.6 cm, at 345° aTDC, port deactivation, k-ε model (color image see on our web site)

As can be seen in figs. 26 and 27 the spatial distribution of kinetic energy of turbulence is more convenient than in the case with simultaneous intake valve opening. Namely, regularly shaped zone of high kinetic energy of turbulence is located in the central part of the chamber and occupies the entire region along z-axis between piston crown and cylinder head. Some initial results related to the effects of turbulence model variation (k-ε and Reynolds stress closure) were already presented in a companion paper [22]. The effects of further turbulence model alteration on the evolution of fluid flow pattern and spatial distribution of kinetic energy of turbulence in 4-valve engine were presented in this paper *i. e.* in figs. 28-39 below. Namely, figs. 28, 31, 34, and 37 are related to standard k-ε model of turbulence while figs. 29, 32, 35, and 38 are related to k-ξ-f model of turbulence. Due to symmetry in x-y plane results for both model of turbulence were presented in the same figure (figs. 30, 33, 36, and 39). In order to alleviate comparisons of fluid flow patterns particularly in the case of turbulence variation the set of subtle different colours were employed as well.

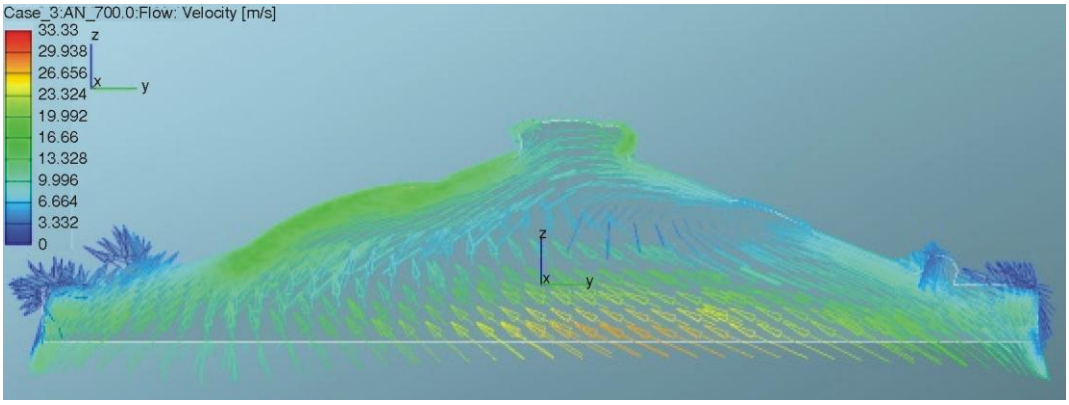

Figure 28. Fluid flow pattern in x-z plane, y = const. at 340 deg. aTDC, k-ε model (color image see on our web site)

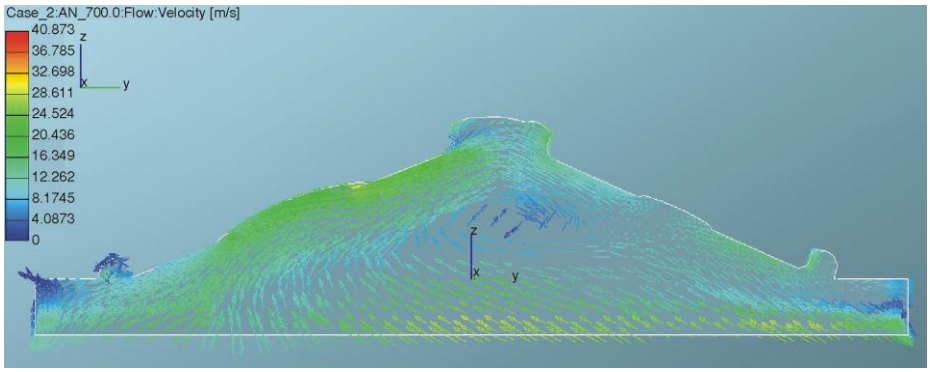

Figure 29. Fluid flow pattern in x-z plane, *y* = const. at 340 deg. aTDC, *k-ξ-f* model (color image see on our web site)

During induction and large portion of compression stroke (up to 270 deg. aTDC) no legible differences as regards the evolution of fluid flow pattern and spatial distribution of kinetic energy of turbulence were observed and therefore not presented due to economy of the paper. The significant differences are commencing in the vicinity of TDC. Namely, the fluid flow pattern and less intensive colours in figs. 29, 32, 30 (right), and 33 (right) than in figs. 28, 31, 30 (left), and 33 (left) indicate less expressive vortex flow and generally smaller velocities in the case of *k-ξ-f* model of turbulence yielding somehow the detention of vortex displacement to the exhaust valve zone thereafter. Larger velocities in the case of *k-ε* model of turbulence are encountered in x-y plane as well (figs. 30 and 33, left).

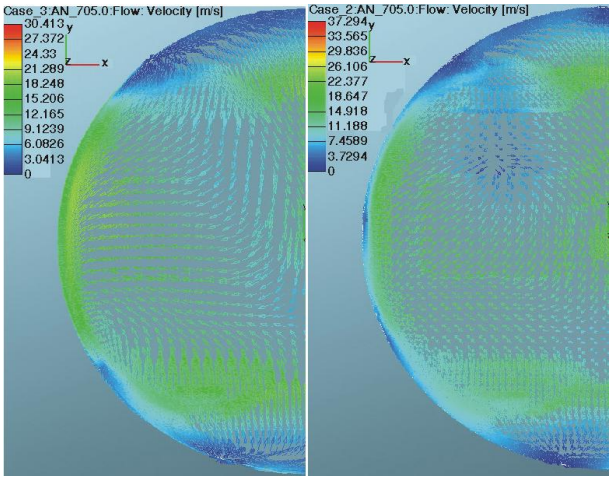

Figure 30. Fluid flow pattern in x-y plane, *z* = const. at 345 deg. aTDC, *k-ε* model (left) and *k-ξ-f* model (right) (color image see on our web site)

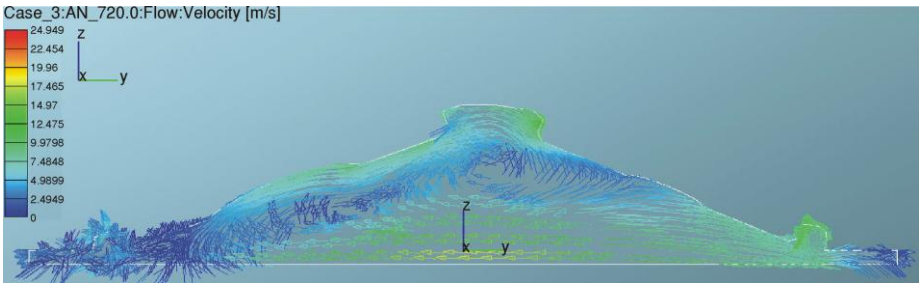

Figure 31. Fluid flow pattern in x-z plane, *y* = const. at 360 deg. aTDC, *k-ε* model (color image see on our web site)

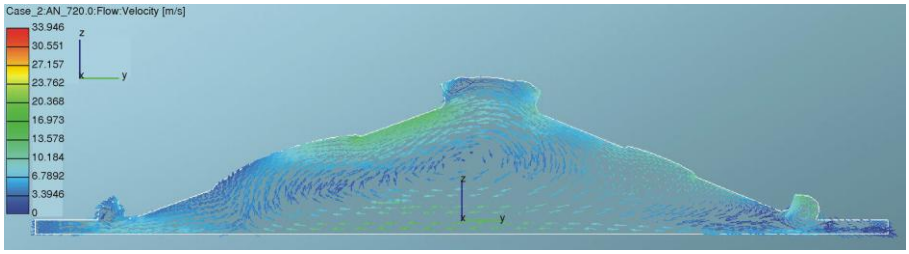

Figure 32. Fluid flow pattern in x-z plane, *y* = const. at 360 deg. aTDC, *k*-ξ-*f* model (color image see on our web site)

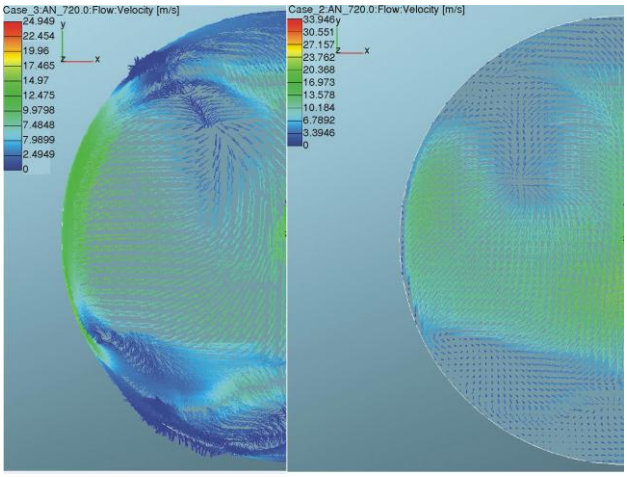

Figure 33. Fluid flow pattern in x-y plane, *z* = const. at 360 deg. aTDC, *k*-ε model (left) and *k*-ξ-*f* model (right) (color image see on our web site)

Differences in fluid flow patterns are pursued in a straightforward fashion by certain differences in turbulence intensity and spatial distribution of kinetic energy of turbulence in all planes. It can be seen that in the case of *k*-ε model of turbulence the maximum kinetic energy of turbulence is located in the central part of the chamber (figs. 34 and 37) while in the case of *k*-ξ-*f* model of turbulence the maximum kinetic energy of turbulence is shifted to the intake valve zone (figs. 35 and 38). In addition, in the case of *k*-ε model, high values of kinetic energy of turbulence prevail and engulf nearly the entire chamber (figs. 36 and 39, left) while in the case of *k*-ξ-*f* model these zones are obviously smaller and akin to characteristic bean-like form (figs. 36 and particularly 39, right). Such a behavior largely affects all other in-cylinder processes that incur such as mixing, combustion, *etc*. In general *k*-ε model of turbulence generates higher values of kinetic energy of turbulence over the broader part of the chamber. Namely, *k*-ε over predicts its value.

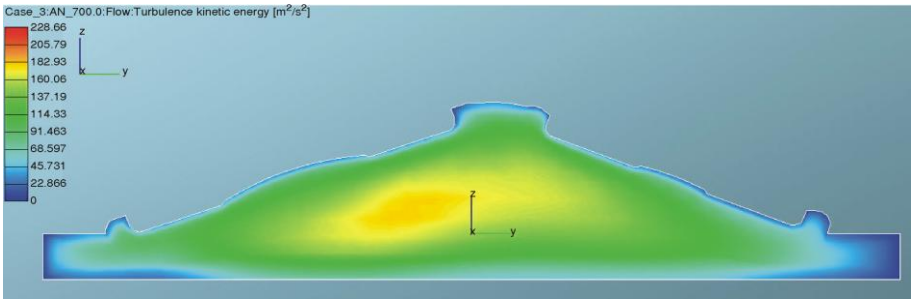

Figure 34. Spatial distribution of kinetic energy of turbulence in x-z plane, *y* = const. at 340 deg. aTDC, *k*-ε model (color image see on our web site)

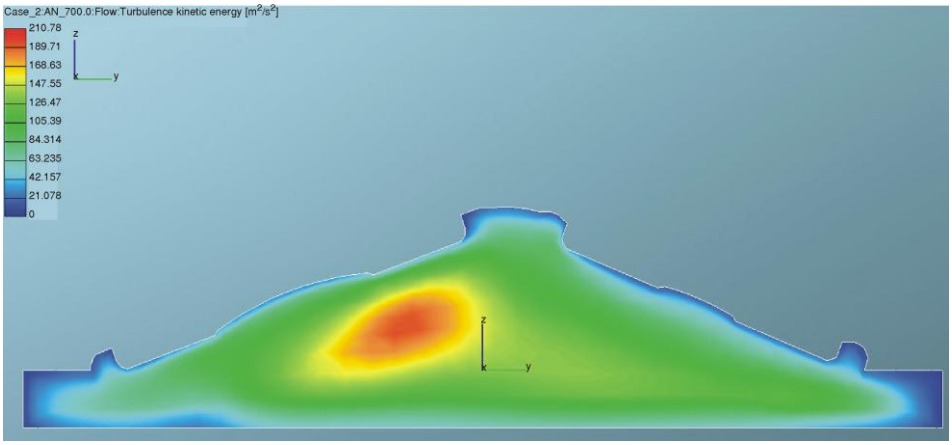

Figure 35. Spatial distribution of kinetic energy of turbulence in x-z plane, *y* = const. at 340 deg. aTDC, *k-ξ̃-f* model (color image see on our web site)

Figure 36. Spatial distribution of kinetic energy of turbulence in x-y plane, *z* = const. at 340 deg. aTDC, *k-ε* model (left) and *k-ξ̃-f* model (right) (color image see on our web site)

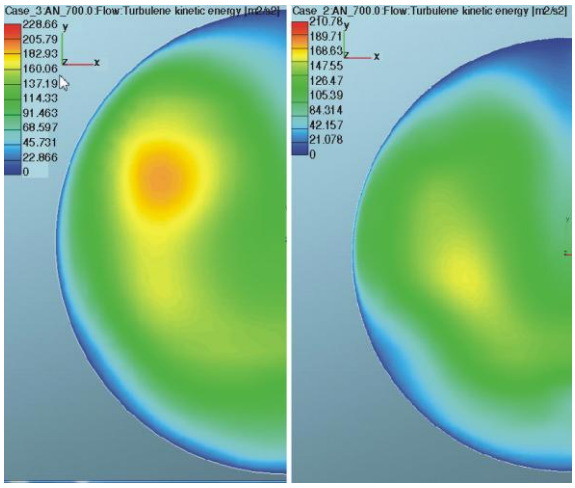

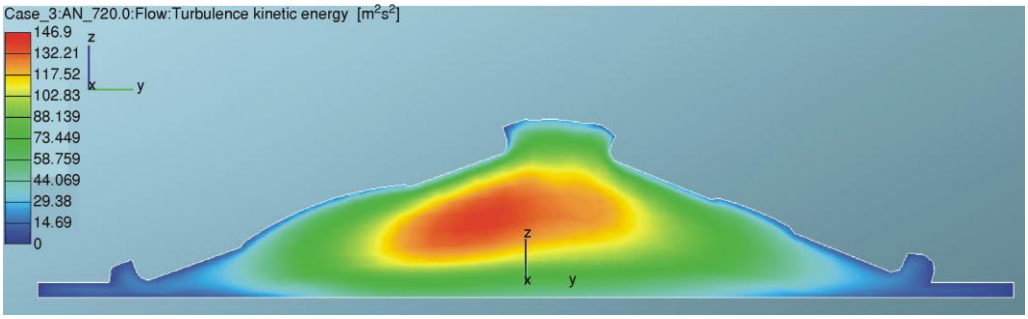

Figure 37. Spatial distribution of kinetic energy of turbulence in x-z plane, *y* = const. at 360 deg. aTDC, *k-ε* model (color image see on our web site)

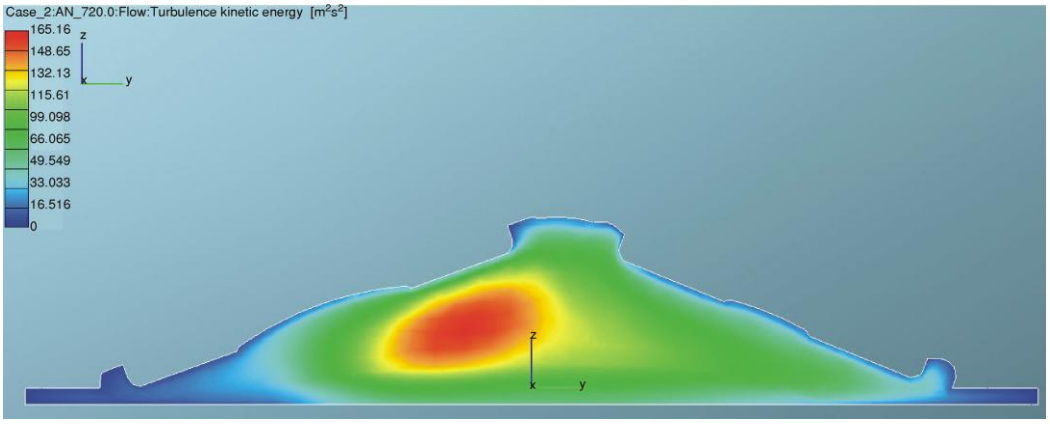

Figure 38. Spatial distribution of kinetic energy of turbulence in x-z plane, *y* = const. at 360 deg. aTDC, *k*-ξ-*f* model (color image see on our web site)

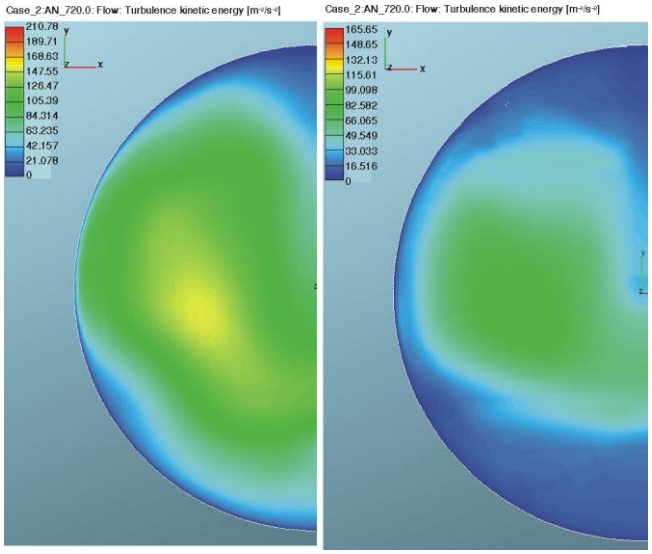

Figure 39. Spatial distribution of kinetic energy of turbulence in x-y plane, *z* = const at 360 deg. aTDC, *k*-ε model (left) and *k*-ξ-*f* model (right)
(color image see on our web site)

Conclusions

The fluid flow pattern during induction and compression in the particular combustion chamber geometry of 4-valve engine is extremely complex and entirely 3-D. In the case with two valves opened tumble motion during induction is clearly legible and followed by gradual deterioration in the vicinity of BDC due to non-uniform distribution along y-axis. During compression strong vortex flow around y-axis and fairly expressive coinciding flow along x-axis in reverse direction is encountered contributing to the inconvenient spatial distribution of kinetic energy of turbulence in the vicinity of TDC. Some benefits concerning generation of swirling flow and better spatial distribution of kinetic energy of turbulence in the vicinity of TDC were gained with port deactivation. Even in the case of the most excessive macro flows such as it is encountered in 4-valve engines the turbulence model variation strongly affects the on-going evolution of fluid flow pattern and spatial distribution of kinetic energy of turbulence. In general *k*-ε model of turbulence generates higher values of kinetic energy of turbulence over the broader part of the chamber than corresponding *k*-ξ-*f* model of turbulence.

References

[1] Danneman, J., *et al*., Cycle Resolved Multi Planar Flow Measurements in a Four Valve Combustion Engine, *Exp.Fluids, 50* (2010), 4, pp. 961-976
[2] Jovanović, Z., Petrović, S., The Mutual Interaction between Squish and Swirl in IC Engines, *Mobility and Vehicle Mechanics, 23* (1997), 3, pp. 72-86
[3] Lee, K., Bae, C., Kang, K., The Effects of Tumble and Swirl Flows on Flame Propagation in a Four-Valve SI Engine, *Applied Thermal Engineering, 27* (2007), 11-12, pp. 2122-2130
[4] Micklow, G. J., Gong, W. D., Intake and in Cylinder Flow Field Modeling of a Four Valve Diesel Engine, *Journal of Automobile Engineering, 221* (2007), 11, pp. 1425-1440
[5] Khaligi, B., Intake Generated Swirl and Tumble Motion in a 4.-Valve Engine with Various Intake Configurations, SAE paper 900059, 1990
[6] Jovanović, Z., Petrović, S., Tomić, M., The Effect of Combustion Chamber Geometry Layout on Combustion and Emission, *Thermal Science, 12* (2008), 1, pp. 7-24
[7] Jovanović, Z., Masončić, Z., Tomić, M., The Vice-Verse Movement of the Reverse Tumble Center of Rotation in a Particular Combustion Chamber, MTM, *International Virtual Journal for Science, Technics and Innovation for the Industry, Year II* (2008), 6-7, pp. 17-20
[8] Masončić, Z., Jovanović, Z., The Effect of Combustion Chamber Geometry Lay-out Variations onto Fluid Flow Pattern, International Automotive Conference with Exhibition, Science and Motor Vehicles, NMV0774, Belgrade, 2007, ISBN 978-86-80941-31-8, pp. 58-67
[9] Markatos, N., *et al.*, Computer Simulation of Fluid Flow and Combustion in Reciprocating Engines, Hemisphere Publishing Corporation, New York, USA, 1989, ISBN 0-89116-392-1
[10] Amsden, A. A., KIVAII: A Computer Program for Chemically Reactive Flows with Sprays, LA-11560-MS, N. Mex., USA, 1989
[11] Amsden, A. A., KIVA3V, Rel.2 Improvements to KIVA3V, LA-UR-99-915, N. Mex., USA, 1999
[12] Amsden, A. A., SALE3D: A Simplified ALE Computer Program for Calculating 3-D Fluid Flows, NUREG-CR-2185, N. Mex., USA, 1981
[13] Yang, S. I., *et al.*, A KIVA Code with Reynolds Stress Model for Engine Flow Simulation, *Energy*, *30* (2005), 2-4, pp. 437-445
[14] Torres, D. J., Trujillo, M. F., KIVA-4: An Unstructured ALE Code for Compressible Gas Flow with Sprays, *Journal of Computational Physics, 219* (2006), 2, pp. 943-975
[15] ***, CFD Solver, AVL FIRE 2009.1
[16] Speziale, C. G., Sarkar, S., Gatski T. B., Modelling the Pressure Strain Correlation of Turbulence – an Invariant Dynamical System Approach, NASA, pp. 1-51, ICASE Report, 1990, 90-5, pp. 1-51
[17] Hanjalić, K., Popovac, M., Hadjiabdic, M., A Robust Near-Wall Elliptic Relaxation Eddy Viscosity Turbulence Model for CFD, *International Journal of Heat and Fluid Flow, 25* (2004), 6, pp. 1047-1051
[18] Durbin, P. A., Near Wall Turbulence Closure Modeling without Damping Functions, *Theoretical Computational Fluid Dynamics, 3* (1991), 1, pp. 1-13
[19] Hanjalić, B. Blending the RANS and LES Concepts for Computing Industrial and Environmental Flows: a Perspective, International Automotive Conference with Exhibition, Science and Motor Vehicles, NMV11AutoSim01, Belgrade, 2011, ISBN 978-86-80941-36-3, pp. 1-9
[20] Basara, B., Pavlović, Z., PANS *vs*. RANS for Computation of the Flow through Intake Engine Ports, International Automotive Conference with Exhibition, Science and Motor Vehicles, NMV11AutoSim09, Belgrade, 2011, ISBN 978-86-80941-36-3, pp. 85-103
[21] Popovac, M., Hanjalić, K., Compound Wall Treatment for RANS Computation of Complex Turbulent Flows and Heat Transfer, Flow, *Turbulence and Combustion, 78* (2007), 2, pp. 177-202
[22] Jovanović, Z., Basara, B., The Controversy Concerning Turbulence Modeling in Automotive Application, M13, PCO Global Conf., Borneo, Malaysia, ISBN 978-983-44483-32, pp. 73-83

Paper submitted: August 25, 2011
Paper revised: August 31, 2011
Paper accepted: September 19, 2011